Catena 190 (2020) 104549

Contents lists available at ScienceDirect

Catena

journal homepage: www.elsevier.com/locate/catena

# Chronostratigraphy of silt-dominated Pleistocene periglacial slope deposits on Mt. Ślęża (SW, Poland): Palaeoenvironmental and pedogenic significance

Jaroslaw Waroszewski[a,*], Tobias Sprafke[b], Cezary Kabala[a], Elżbieta Musztyfaga[a], Aleksandra Kot[a], Sumiko Tsukamoto[c], Manfred Frechen[c]

[a] Wroclaw University of Environmental and Life Sciences of Soil Science, Department of Soil Science and Environmental Protection, Grunwaldzka 53, 50-357 Wroclaw, Poland
[b] University of Bern, Institute of Geography, Hallerstrasse 12, CH-3012 Bern, Switzerland
[c] Leibnitz Institute for Applied Geophysics (LIAG), Department of Geochronology, Stillweg 2, 30655 Hannover, Germany

ARTICLE INFO

*Keywords:*
Quaternary
Pedogenesis
Loess
Slope sediments
OSL dating

ABSTRACT

Slope deposits with aeolian silt admixture are a widespread parent material of soils in the temperate zone but may be neglected when rates of soil production are quantified. The concept of periglacial cover beds differentiates slope deposits with or without aeolian silt admixture; yet there is a remaining debate on processes and the timing of their formation. A previous study done by us at Mt. Ślęża, SW Poland, concluded that slope deposits with variable aeolian silt admixture, or its lack, have a significant influence on the pathway of soil formation. The present work builds upon this finding, by adding further granulometric and micromorphological data from three representative profiles along a toposequence, in order to refine our understanding of local slope deposits and soil formation. Additionally, seven numerical ages using luminescence dating provide a chronological framework for our reconstructions and allow linking the forming processes of these pedosedimentary records to regional palaeoenvironmental conditions. The oldest aeolian deposits are of Middle Pleistocene age (> 280 ± 19 ka) with interlayered palaeosol (marine isotope stage [MIS] 9 or older). Late Pleistocene slope deposits encompass the maximum loess thickness and are dated to MIS 2. Luminescence ages from the upper layers indicate shallow reworking, which we tentatively correlate to the Younger Dryas (YD). Two profiles with thick loess mantles have strong clay illuviation features, presumably formed during the Holocene. However, weak clay illuviation in the third profile with a thin loess mantle (having an age of YD) over granite regolith seems to have occurred before the Holocene, as only fragmented clay coatings (probably MIS 2 pedogenesis) could be found.

## 1. Introduction

Soil as living skin of the earth provides numerous services to nature and society. However, rates of soil formation are subject of ongoing debate as quantitative estimates often rely on steady-state assumptions (Phillips, 2010; Stockmann et al., 2014). Periglacial slope sediments are considered as main parent material for soils in hilly and mountainous environments of the temperate zone, which have not been covered by ice during the last glacial period (Kleber and Terhorst, 2013, Kleber et al., 2013). Significant aeolian silt additions to periglacial slope sediments have gained increasing recognition in respect to soil formation (Kleber, 1997; Kleber and Terhorst, 2013; Waroszewski et al., 2013, 2018a; Martignier et al., 2015; Veit et al., 2017; Gild et al., 2018; Döhler et al., 2018; Loba et al., 2020). Aeolian silt admixture to slope deposits has variable quantity and these deposits vary in their thickness and stratigraphy, which influences the edaphic conditions and pathways of soil formation (Mailänder and Veit, 2001; Büssemer, 2002; Lorz et al., 2013, Waroszewski et al., 2018b). Such pedosedimentary sequences provide important climatic and environmental proxies and helped to define timeframes of soil development (Constantini and Priori, 2007; Zerboni et al., 2014).

In temperate humid environments of central and northern Europe, aeolian coarse silt is an excellent paleoenvironmental marker linked to glacial conditions. Several researchers differentiate an “upper layer” and an “intermediate layer”, both with significant dust admixture to local substrate from a “basal layer” that consists entirely of local material (Semmel and Terhorst, 2010, Kleber and Terhorst, 2013). It has been a long-held view, that the upper layer corresponds to the Younger

* Corresponding author.
*E-mail address:* jaroslaw.waroszewski@upwr.edu.pl (J. Waroszewski).

https://doi.org/10.1016/j.catena.2020.104549
Received 30 November 2019; Received in revised form 4 March 2020; Accepted 6 March 2020
Available online 20 March 2020

Dryas (Semmel and Terhorst, 2010), whereas for intermediate and basal layers both Middle to Late Pleistocene ages are probable (Kleber et al., 2013. So far the studies on the slope deposits (cover beds) on mountain slopes in Poland were mainly descriptive (Kacprzak and Derkowski, 2007; Migoń and Kacprzak, 2014; Waroszewski et al., 2018b; Kowalska et al., 2019), or relied only on $^{14}$C dating and palynological analyses (Waroszewski et al., 2013, 2018a) to establish approximate time frames of cover bed formation. Both, the Lake Laach Tephra (ca. 12.9 ka, e.g.; Schmincke, 2006), a widely used stratigraphic marker horizon in Germany, and organic interbeddings, useful for $^{14}$C dating, are absent in the area under study.

In the last decades, luminescence dating led to remarkable advances in understanding terrestrial palaeoenvironmental records. Luminescence chronologies of cover beds are yet scarce, but those that are published from different regions of Central Europe (Kleber et al. 2013, Veit et al. 2017) partly question the established chronostratigraphic schemes for cover beds. Aeolian silt to fine sand is typical for upper and intermediate layers and very suitable for luminescence dating (Roberts, 2008). As silt is highly erodible, silty soils are susceptible to reworking along slopes, creating downslope records of colluvial materials, which are suitable for luminescence dating (Fuchs and Lang, 2009). Precision in dating meets many difficulties with periglacial slope deposits, as aeolian deposits are mixed with the local substrate by frost dynamics and transported downslope by solifluction (Hülle et al. 2009, Kleber et al. 2013, Döhler et al. 2018). Furthermore, bioturbation affects soils and surficial deposits, which complicates the interpretation of luminescence data (Reimann et al., 2017).

To overcome the controversies related to the chronostratigaphic significance of cover sediments, more research including a larger number of luminescence ages from different regions and landscape contexts is required. This will contribute to a deeper understanding of the complex forming and overprinting mechanisms of slope deposits as parent materials for soils of the temperate zone. Qualitative models of polygenetic soil profile evolution that include phases of morphodynamic stability and activity (Sprafke et al. 2014; Sprafke, 2016; Waroszewski et al., 2018b) are a prerequisite to quantify rates of pedogenesis (Waroszewski et al., 2018a).

Until now, no comprehensive chronology of slope covers with significant aeolian silt contribution is available from Eastern Central Europe. The main aim of this research is to evaluate genesis and time span of slope deposits formation on a well-studied toposequence at Mt. Sleza, Lower Silesia, SW Poland. Micromorphological observations and several luminescence ages complement previously published morphological, granulometric and geochemical data (Waroszewski et al. 2018b). In addition, high-resolution particle size distribution (PSD) data will be presented from each horizon measured by laser diffraction in order to identify the main modes in the PSD. Herein, we discuss the possible palaeoclimatic conditions that led to aeolian and colluvial processes or resulted in phases of pedogenesis.

## 2. Materials and methods

### 2.1. Study area

The study area was characterized in detail by Waroszewski et al. (2018b). The transect under investigation is located between 248 and 265 m a.s.l. at the western footslope of Mt. Ślęża (715.5 m a.s.l.). There, the local geology is made up of Variscinian granitoids, whereas further upslope gabbro predominates in the upslopes (Kryza and Pin, 2010). Quaternary sediments of variable thickness like glacial tills and glaciofluvial sands of the Middle Pleistocene glaciations (Fig. 1) were found up to 550 m a.s.l. (Hall and Migoń 2010). Loess and loess-like deposits, mainly deflated from the Great Odra River valley (Badura et al., 2013), reach up to 300 m a.s.l. and are mostly of the Late Pleistocene age (Jary et al., 2002; Waroszewski et al., 2018b). The Księginice profile, located few kilometers SE of Mt. Ślęża, is one of few sites in the region, where greater than 2 m thick loess sediments were reported (Kida, 1999).

Slopes at the Mt. Ślęża have very variable length and microrelief mostly due to petrographic differentiation and variable resistance to weathering (Migoń, 1997). In addition, there is a complex pattern of remnants of cryoplanation terraces, fine-grained solifluction deposits and coarse block covers (Żurawek, 1999). Luminescence ages of glaciofluvial sands presumably incorporated into a rock glacier (Żurawek, 2001) date to Late Middle Pleistocene (264–387 ka) and are the only yet available chronostratigraphic data from sediments in the study area.

The upper slopes of Mt. Ślęża are dominated by Leptosols and Cambisols formed from slope deposits (Kabala and Jezierski, 2011; Pędziwiatr et al., 2018) that were not or very weakly affected by aeolian silt deposition (Waroszewski et al., 2018a). In the mid- to footslope, the distribution of Cambisols, Skeletic Luvisols/Alisols, Stagnic Luvisols and Retisols is mainly controlled by the thickness of aeolian mantles and the degree of aeolian silt admixture (Waroszewski et al., 2018a). In the lowlands around Mt. Ślęża Chernozems, Phaeozems or Luvisols are mainly a function of past land use (Kabała et al., 2019; Labaz et al., 2018, 2019a; Łabaz et al., 2019b; Kabala et al., 2015).

### 2.2. Field description and sampling

Three soil profiles (S2, S3, S4) from a previous study by Waroszewski et al. (2018b) are developed from different types of periglacial slope sediments and show variable intensities of the morphological features/diagnostic horizons (e.g. clay illuviation) (Table 1). Descriptions based on sedimentological and pedological properties follow the Guideline for soil description (2006) and soil classification was done according to the WRB system (IUSS Working Group WRB, 2015). Among investigated soils specific layers were distinguished: aeolian mantle, mixed zone and basal layer, referring to way of profiles evolution due to different contribution of aeolian silts. For detailed field and analytical characteristics and conditions of formation above-mentioned layers please see Waroszewski et al. (2018b) and Waroszewski et al. (2019).

Soil color was estimated in the field on moist samples with Munsell Soil Colour Charts. Samples for physical and chemical analyses are from each horizon. Seven samples for luminescence dating were taken from selected layers by hammering steel tubes into the freshly cleaned outcrop walls (positions in Fig. 2). Undisturbed (with preserved soil structure) soil material for micromorphological investigations was sampled from four selected soil horizons in total (please see subchapter 3.3. Micromorphological features of soils) using Kubiena boxes (6 × 4 cm). Disturbed samples for soil analyses were air dried, gently ground, and passed through a 2 mm sieve.

### 2.3. Particle size analyses

A Beckman–Coulter LS 13,320 PIDS laser diffraction at LIAG Hannover measured the particle sizes distribution (PSD) between 0.04 and 2000 μm after dispersion of the samples for 12 h on a rotator using 1% ammonium hydroxide. Laser diffraction has a high spectral resolution (116 classes) and allows the detection of separate modes in PS distribution, which may reflect different sediment sources or a mixing of substrates (Schaetzl & Luehmann, 2013). Appearance of subordinate modes within the general pattern can be related to measuring artefacts of the laser diffraction device and should be interpreted with special caution (Schulte et al., 2018). Determinations for fine particles differ from classical methods, therefore absolute estimates of clay contents may require adaptions of the silt/clay boundary (Konert and Vandenberghe, 1997). Particle size distribution from the studied profiles, based on the hydrometer-sieve method (van Reeuwijk, 2002), are available from a previous study (Waroszewski et al., 2018a). Herein, we refer specifically to the location of modes within the sand and silt fractions.

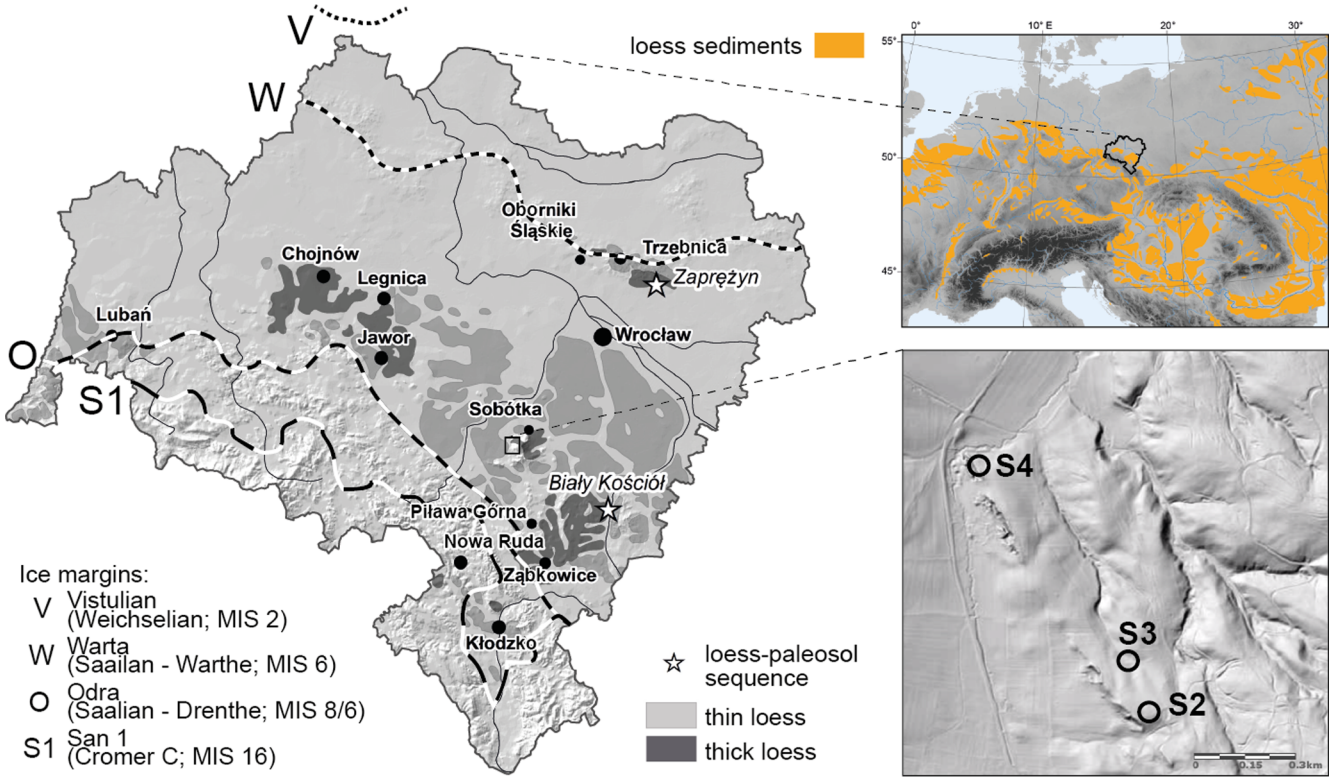


**Fig. 1.** Location of the studied sites in the Lower Silesia region. Note the mapped loess distribution of Lower Silesia (Waroszewski et al., 2018a) within the European loess belt (map of loess sediments in Central Europe adapted from Sprafke 2016, after Haase et al. 2007). Thick loess deposits refer to sediments having thickness > 2 m, while thin loess > 2 m. DEM model shows main relief of slopes and location of soil profiles.

### 2.4. Luminescence dating

All sample preparations for luminescence dating were conducted under subdued red-light condition. The sample material from outer ~1 cm of both sides of the tubes, which might have been exposed to light, was discarded. The material from the inner part of the cylinders was treated with 10% hydrochloric acid to dissolve carbonates, 3% sodium oxalate to separate aggregates and 30% hydrogen peroxide to remove organic matter. The fine silt size fraction (4–11 μm) was separated by sedimentation based on Stokes law (Frechen et al., 1995). The prepared polymineral fine grains were settled onto aluminum discs (~2 mg/disc) from a suspension in distilled water.

The annual dose rates of the samples were determined by radioactivity measurements using high resolution gamma spectrometry. The sample material for dosimetry was dried at 130 °C, and 700 g of each sample was packed and stored in Marinelli beakers for at least four weeks to establish equilibrium between radon and daughter nuclides before the measurements with a N-type high purity germanium detector. The concentration of U, Th and K was calculated from the measured gamma activities. The total dose rates were calculated using the conversion factors of Guérin et al. (2011) and the cosmic dose rate based on Prescott and Hutton (1994). A water content of 20 ± 10% was assumed based on the natural water content, except sample LUM3613 for which a water content of 5 ± 5% was assumed. For alpha efficiency, an a-value of 0.08 ± 0.02 was used (Rees-Jones, 1995).

All luminescence measurements were done with a Risø DA-20 TL/OSL reader equipped with a calibrated $^{90}Sr/^{90}Y$ beta source (~0.1 Gy s-1). Feldspar luminescence signal from the polymineral fine grains was stimulated with infrared (IR) LEDs (at 870 nm, 110 mW) and detected using a combination of detection filters in the blue/UV wavelength (BG39 and Corning 7–59; 380–460 nm). The post-IR IRSL protocol with an elevated stimulation at 225 °C for 200 s with a prior IR stimulation at 50 °C for 100 s (thereafter $pIRIR_{225}$ protocol; Thomsen et al., 2008) was employed for the equivalent dose ($D_e$) measurements using the single aliquot regenerative dose (SAR) method (Murray and Wintle, 2000). Six aliquots for each sample were used and mean $D_e$ values with one sigma standard error were calculated.

The performance of the $pIRIR_{225}$ protocol was checked by the recycling ratio and dose recovery tests (Murray and Wintle, 2000; 2003). To test the validity of the sensitivity correction in the $pIRIR_{225}$ SAR protocol (the recycling ratio test), a same regeneration dose was given twice at the beginning and end of, and the ratio of the two luminescence intensities after sensitivity correction was calculated. For the dose recovery test, six aliquots of each sample were bleached in a solar simulator (Hönle SOL2) for four hours. The residual dose after bleaching was measured using three of the six aliquots using the $pIRIR_{225}$ protocol. The remaining three bleached aliquots per sample were irradiated by a beta dose, which was approximately equal to the natural dose, then the dose was measured with the SAR protocol to test if the given dose can be recovered. The recovered dose minus the residual dose was compared with the given dose.

Anomalous fading (Wintle, 1973) of the $pIRIR_{225}$ signal was measured following Auclair et al. (2003) using three aliquots per sample. For samples LUM3611, 3614, 3618, 3619, and 3620, the fading uncorrected ages, which were obtained by dividing $D_e$ by the dose rate, were corrected using the method of Huntley and Lamothe (2001). For the remaining two older samples (LUM3612 and 3613), the Huntley and Lamothe (2001) method cannot be used, therefore we used the correction method of Lamothe et al. (2003) to calculate fading corrected ages. Recently, this fading correction method was confirmed to yield consistent fading corrected ages as the more widely accepted method of Kars et al. (2008), if a g-value is less than ~4%/decade (Li et al., 2018). After the fading correction, the minimum depositional ages were calculated based on 2 times characteristic saturation dose ($D_0$) of the dose response curve (Wintle and Murray, 2006).

**Table 1**
Soil sites characteristics.

| Soil profile | Elevation (m a.s.l.) | Latitudes/ longitudes | Position in landscape/slope relief | Exposure | Slope (°) | Geological substrates | Type of land use | Soil type (WRB, 2015) |
|---|---|---|---|---|---|---|---|---|
| S2 | 265 | 50°52′12.7″/ 16°40′34.4″ | midslope/convex | NW | 4 | loess/fluvioglacial deposits/eolian sand/granite | grassland | Stagnic Luvisol (Cutanic, Raptic, Ochric, Siltic) |
| S3 | 248 | 50°52′16.4″/ 16°40′33.2″ | midslope/concave | NW | 10 | loess | grassland | Eutirc Stagnic Retisol (Cutanic, Ochric, Siltic) |
| S4 | 260 | 50°52′35.0″/ 16°40′09.1″ | summit/shoulder | NE | 2 | loess/granite | forest | Endoskeletic Alisol (Cutanic, Ochric, Raptic, Siltic) |

### 2.5. Soil micromorphology

Undisturbed samples were saturated in an Epovac (Struers vacuum chamber) with Polimal 108 polyester resin. Dried impregnated rectangular cubes were cut with a Struers® saw into small slides, mounted on glass slides and lapped and polished with CL50 (Logitech®) to 25–30 μm thickness. Microscopic observations of thin sections were done using a Nikon Eclipse 400 microscope, in both plane and cross-polarised light. Each thin section was described according to the terminology of Stoops (2003). The description of a thin section includes microstructure and arrangement of the voids; detailed analysis of groundmass (c/$f_{5\mu m}$-related distribution pattern, b-fabric) as well as pedofeatures with strong emphasis on forms of clay illuviation (Table 5).

## 3. Results

### 3.1. Soil morphology and slope deposits characteristics

Profile S3 represents thick loess-derived deposits practically free of coarse fragments (Fig. 2, Table 2). The profile can be subdivided into three layers, with the uppermost consisting of loess colluvium. This layer has a thickness of 40 cm and a granular/angular structure. It contains individual brick pieces and charcoal and is separated with a mostly clear wavy boundary from the underlying layer. Some colluvium material is incorporated into the uppermost part of the Eg/Btg horizon. This second unit comprises loess with clear clay illuviation features (medium on the surface of soil peds, ca. 20–30%) and silty wedges of bleached material. Silty tongues break through the argic horizon and have usually 2–3 cm of diameter. Larger wedges of ca. 40–80 cm long appear in the central part of the profile, in Eg/Btg and Btg/Eg horizons. Some of them have clear biogenic origin evidenced by their root-like shape (Fig. 2). The third layer in the bottom of the profile is developed from laminated loess (> 65 cm thick) with a microstratification. In the C3 horizon a noticeable share of fine/medium sand has been detected.

Profile S4 consists in the upper part of a 30(−50) cm thick loess mantle, hosting the ABw and Bw horizons featured by subangular and angular blocky structure and low content of coarse granite fragments (5–10%), present mostly close to the wavy border of the layer (Fig. 2). Biogenic alteration of structure and colour are typical for the cambic horizon. The loess mantle transitionally passes into a layer composed from loess and granite regolith, with clear geochemical signal of aeolian silt (Waroszewski et al., 2018a; Fig. 3). Soil substrate in this mixed zone is arranged into angular blocky and platy aggregates. Features of clay accumulation (silt–clay coatings) are very poorly to poorly developed on soil aggregates and rock fragments. The content of angular rock fragments increased rapidly into 40–60% in the 2Bt horizon. The lowermost section, starting from the depth of 70 cm, contains 70–85% of angular rock fragments, arranged typically for granite regolith ('grus'). The texture class of fine earth particles in this layer is sandy loam.

Profile S2 has the most complex stratigraphy (Fig. 2). The uppermost 70 cm is a loess mantle. Within the first 40 cm (AEg and Eg horizons) some reworking features are very obvious: a friable consistency and a wavy boundary to the underlying layer. Below the Eg horizon the structure changes into angular/platy and platy and the consistency becomes more firm. Aggregate surfaces and root channels are covered with clay skins. Redoximorphic mottles and discontinuous cracks are common. Cracks cover ca. 20% of the Btg horizon and have glossic features.

The loess mantle passes abruptly into strongly compacted glaciofluvial material (2Btg) with a well-developed platy/angular structure. This horizon contains 50–60% of gravels and stones (including Scandinavian granites) and reveals very intense clay accumulation expressed by reddish (5YR 4/5) and red-yellowish (7.5YR 5/8) coatings. The 2Btg horizon is clearly separated from the underlying silty-textured 3Btg horizon (common clay coatings) with numerous thin cracks filled

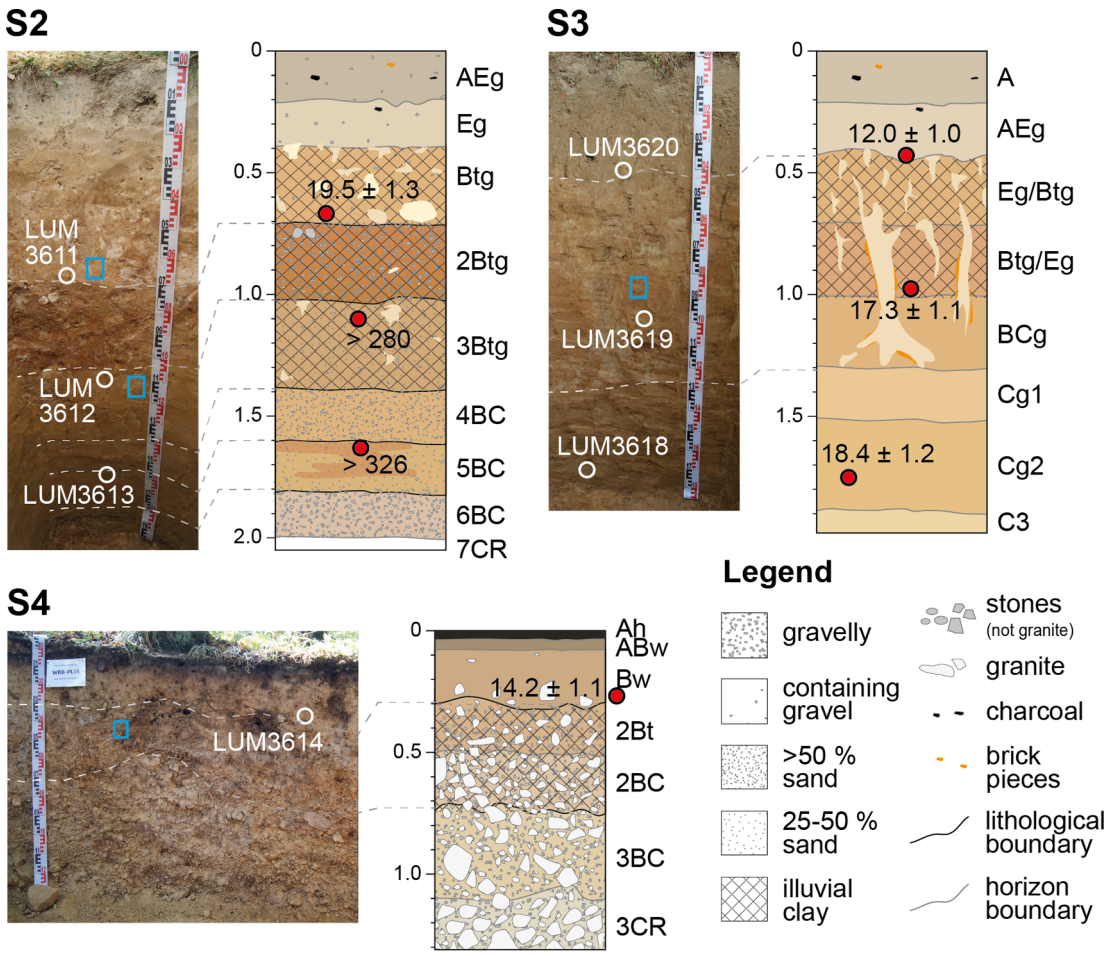


**Fig. 2.** Photos and sketches showing the detailed morphology of all presented soils profiles and sampling position for OSL analyses with obtained ages. Blue rectangles marked micromorphological samples position. (For interpretation of the references to color in this figure legend, the reader is referred to the web version of this article.)

with bleached material (10YR 7/1), identified as retic property. From the depth of 139 cm, the silty material changes into sandy (medium sand) with redoximorphic reddish mottles. The structure is subangular and weak, very thin tonguing appears here. Between 160 and 200 cm again silty material appears with a variable content of granite fragments that increases with depth. The whole profile ends with granite regolith (horizon 7CR). Identified tongues (in Btg and 3Btg) appear independently in soil horizons and do not form one structure throughout the whole soil profile.

### 3.2. Particle size distribution of studied soils

The results of laser diffraction analysis are shown as heatmaps (Schulte et al., 2016) to visualize the whole dataset and show the main modes in particle-size distribution of soils (Fig. 3), including the lithological differentiation of particular layers. The aeolian mantle in profile S2 shows a distinct coarse silt mode (30–38 μm), with the topmost horizon enriched in sand fraction. The 3Btg and 5BC horizons also show silt dominance, with slightly coarser modes (42 and 46 μm, respectively). The 6BC marks the transition to the granite regolith (7CR) dominated by coarse sand at the base of the section. The glaciofluvial unit (2Btg) and the sand layer intercalating the lower two silt loams are dominated by sand with a mode in medium (414 μm) to fine (140 μm) sand, respectively. A secondary weak mode is expressed at 6 μm, in the fine-medium silt fraction of the 2Btg horizon.

Profile S3 has a coarse silt mode throughout the profile with a variable admixture of sand in the two topmost and the lowermost horizons. In the lower half of the profile the grain size mode is closer to fine sand (40–42 μm), in the upper half it moves successively towards medium silt (24–26 μm in the A and AEg horizons). The aeolian mantle in S4 has a clear peak in the coarse silt fraction (mode: 38–41 μm) and a significant sand component. The mixed zone below has its main modes in the coarse sand (main: 1064, secondary: 525 μm) and subtle peaks in the silt fraction (2Bt: 44 μm, 2BC: 8 μm). There is no distinct silt mode in the lowermost horizon of this profile.

### 3.3. Micromorphological features of soils

Analyzed four illuvial horizons (profile S2 Btg, 3Btg; profile S3 Btg/Eg; profile S4 2Bt) have several common characteristics (Table 5). The prevailing coarse and fine silt is composed of quartz and feldspars whereas finer particles are mainly composed of clay minerals (Figs. 4, 5). The microstructure in Bt horizons of S2 and S3 profiles is subangular blocky and accompanied with regular and star-shaped vughs, while the 2Bt horizon of profile S4 is mostly crumby. The b-fabric of all samples is mostly speckled (Fig. 4a-h, 5a-d) and randomly-striated (Fig. 5e-h).

The most prominent pedofeatures are non-laminated and micro-laminated clay coatings, among them humus (e.g. Fig. 4a-c), limpid (e.g. Fig. 4g, 5a) and dusty clay (e.g. Fig. 4a, 4 g, 5e-f) but also anorthic nodules (Fig. 5). The best developed clay coatings were recognized in the Btg, 3Btg horizons of profile S2 and Btg/Eg of profile S3. Between them few differences were observed. In the Btg horizon of profile S2 humus clay coatings (black/dark brown) are alternating with dusty clay coatings (brown-reddish) and orange-yellowish limpid clay coatings

**Table 2**
Profiles morphology.

| Soil horizon | Depth (cm) | Color (moist) | Structure (type, degree) | Texture class | Horizon boundary | $CaCO_3$ | Clay skins | Diagnostics | Parent material |
|---|---|---|---|---|---|---|---|---|---|
| Profile S2 | | | | | | | | | |
| AEg | 0–21 | 10YR 4/3 | sa, m | SiL | c, w | – | – | | loess |
| Eg | 21–40 | 10YR 5/3 | sa, m | SiL | g | – | – | | loess |
| Btg | 40–70 | 10YR 5/6 | ab, m | SiL | c | – | + + | argic | loess |
| 2Btg | 70–100 | 7.5 YR 5/9 | ab/pl, m | SL | c | – | + + + | argic | fluvioglacial sediment |
| 3Btg | 100–139 | 10YR 5/6 | pl/ab, m | L | c | – | + + | argic | loess |
| 4BC | 139–160 | 10YR 5/8 | sb, f/m | SL | c | – | – | | eolian sand |
| 5BC | 160–180 | 10 YR 5/6 | sa, m/c | L | c | – | – | | loess |
| 6BC | 180–200 | 2.5 YR 6/6 | sa, m | L | c | – | – | | loess/granite |
| 7CR | 200+ | – | – | S | – | – | – | | granite regolith |
| Profile S3 | | | | | | | | | |
| A | 0–20 | 10YR 5/3 | g, f/m | SiL | c, w | – | – | | loess |
| AEg | 20–40 | 10YR 5/4 | ab, m | SiL | c, w | – | – | | loess |
| Eg/Btg | 40–70 | 10YR 5/6 | ab, m | SiL | g | – | + + + | argic | loess |
| Btg/Eg | 70–100 | 7.5YR 5/6 | ab/pl, m | SiL | g | – | + + + | argic | loess |
| BCg | 100–130 | 10YR 5/6 | ab, m | SiL | g | – | – | | loess |
| Cg1 | 130–150 | 10YR 6/6 | ab, m | SiL | g | – | – | | loess |
| Cg2 | 150–190 | 10YR 5/6 | ab, m | SiL | g | – | – | | loess |
| C3 | 190+ | 10YR 6/4 | sa, m | SiL | – | – | – | | loess |
| Profile S4 | | | | | | | | | |
| Ah | 0–3 | 7.5YR 2.5/1 | g, f | SiL | c | – | – | | loess |
| ABw | 3–8 | 7.5YR 4/5 | g, m | SiL | g | – | – | | loess |
| Bw | 8–30 | 10YR 5/6 | sa, m | SiL | g | – | – | cambic | loess |
| 2Bt | 30–50 | 10YR 6/5 | ab, m | SiL | c, w | – | – | cambic | loess/granite |
| 2BC | 50–70 | 10YR 6/4 | pl/ab, m/c | SiL | g | – | + | argic | loess/granite |
| 3BC | 70–110 | 7.5YR 5/8 | ab, m | SL | g | – | – | | granite regolith |
| 3CR | 110–130 | – | – | SL | – | – | – | | granite regolith |

Explanations:
Abundance of clay and $CaCO_3$ accumulation: none (–), weak (+), moderate (+ +), strong (+ + +).
Types of structure: g – granular, ab – subangular blocky, sa – subangular and angular blocky, sb – subangular blocky, pl – platy.
Horizon boundary: c – clear, g – gradual, w – wavy.

(Fig. 4 a-d). Among these, a large number of well-oriented clay coatings with moderately clear extinction bands was noted. Also, in illuvial horizon (Btg/Eg) of profile S3 dusty clay brown-reddish coatings appear with limpid orange-brown clay coatings and dark humus coatings, in similar intensity throughout the groundmass, while in the 3Btg horizon of profile S2 the abundance of clay coatings is much smaller, and they are also much less orientated. Clear layering of dusty and limpid clay coatings in argic horizons of S2 and S3 profiles suggests two phases of clay illuviation. In profile S4 (2Bt horizon) clay illuviation features are rather poorly developed, here mostly very dusty dark brown-orange clay coatings dominate, whereas humus clay coatings are present but very rare. Some larger coatings are very weakly laminated, almost all coatings are partially or weakly fragmented (Fig. 5 e-h) and distributed throughout soil mass. No features typical for colluviation, solifluction transformation or other frost action processes were noted in studied thin sections.

### 3.4. Reliability of luminescence ages

The dose rates are summarized in Table 3. The recycling ratios were within 10% of unity for all measured aliquots and therefore satisfactory. The measured to given dose ratio were all within 10% from unity, ranged between 0.91 ± 0.01 and 0.96 ± 0.03, indicating that the applied SAR protocol can reliably measure the $D_e$ of samples. The fading rate ($g_{2days}$ value) was between 1.04 ± 0.16 and 2.57 ± 0.22%/decade. The $D_e$ values, fading uncorrected and corrected ages are given in Table 4. The two samples (LUM3612 and 3613) showed that the natural $pIRIR_{225}$ signal were in saturation after the fading correction. Thus, the minimum depositional ages were calculated. (see Table 4)

## 4. Discussion

### 4.1. Slope deposits

The studied slope deposits consist purely or partly of allochthonous material, which excludes soil formation directly from weathered bedrock (Waroszewski et al., 2018b). Of the three investigated profiles S3 shows comparably little variation in grain size distribution. Here, a stagnic Luvisol developed from loess (Fig. 3) of sufficient thickness to host the whole soil profile, typical for Central European loess landscapes under atlantic influence (Kabala et al., 2015). Sand enrichment and a partly layered appearance observed in the lower part of the profile (Cg3) are typical for loess sediments which were reworked by slope wash processes, similar to microlaminated 'Schwemmlöss' (Techmer et al. 2006; Döhlert et al., 2018). The slight shift of the grain size mode to finer fractions, still within the boundaries of the coarse silt, can have both sedimentary and pedogenic reasons; e.g. reduced windspeed or post-sedimentary transformations, respectively. The lower hafnium (Hf) concentration and higher sand contents of the AEg horizon (Fig. 3) and the presence of charcoal could be interpreted as indicators for a colluvial origin of these horizons.

The upper 70 cm of Profile S2 consist of a loess mantle overprinted by soil formation with a comparable morphology to the upper part of profile S3. Below 70 cm there are marked changes in both lithology and pedogenic features that testify the polygenetic origin of this pedosedimentary sequence. Remnants of silty, sandy, and at the bottom of the section gravelly sediments overprinted by pedogenesis cover strongly weathered granite saprolite. The sharp contrast between the 2Btg and 3Btg horizons relates to an erosional phase before deposition of sandy to gravelly/stony substrate interpreted as reworked glaciofluvial sediment by Waroszewski et al. (2018a). Profile S4 differs strongly in its morphology from S2 and S3. Only the upper 30 cm shows a clear coarse silt mode typical for local loess sediments. Below 70 cm there is no distinct silt mode and Hf content is significantly lower, excluding

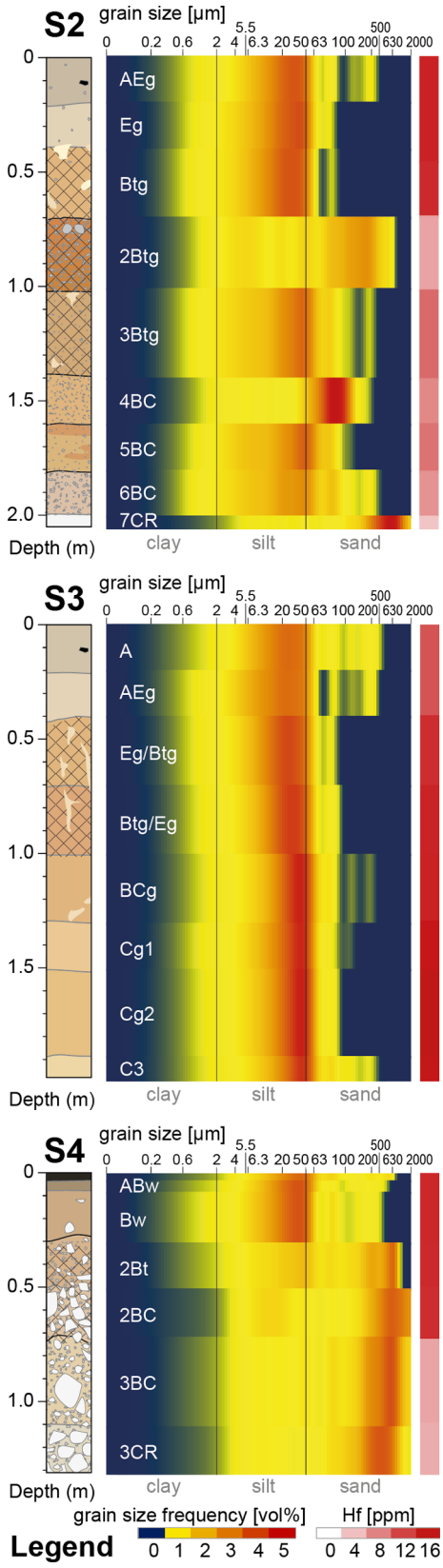


**Fig. 3.** Grain size distribution in studied profiles.

aeolian contribution to the lower part of the profile (Fig. 3).

Multiple phases of loess deposition and reworking processes result in the formation of a complex system of slope deposits on Mt Ślęża. Next to the Schwemmlöss of profile S3, we detect periglacial cover beds (Kleber and Terhorst, 2013); however, their classification is not straightforward. Basal layers (LB) made up of local granite regolith, partly reworked and without dust admixture are present in the lower part of profile S4 and S2. The 40 cm thick middle part of profile S4 made up of local granite regolith and with an aeolian dust admixture corresponds to an intermediate layer (LM). The LM in profile S2 corresponds to the horizons between 40 and 70 cm. An upper layer (LH) makes up the upper 40 cm of S2 (A and E horizons), which is similar to the upper 40 cm of profile S3. In both positions these horizons appear bioturbated and ploughed. LH in profile S4 has a comparable thickness (ca. 30 cm) but based on the morphology we assume it developed by gravity-driven geomorphic processes and/or frost acting processes (few sharp and disoriented granite fragments directly above boundary with the intermediate layer).

### 4.2. Chronology

Dating slope covers with optical luminescence is a promising approach to derive reliable chronologies for their formation. However, in Poland luminescence methods for dating slope deposits with variable aeolian silt admixture were very rarely used and this is the first attempt to date silt dominated slope deposits. The heterogenous composition of slope covers, short-range transport and bioturbation result in several methodological problems (Kleber and Terhorst, 2013). The main difficulties with luminescence dating of periglacial slope deposits are related to the incomplete bleaching of quartz and feldspar grains during sunlight exposure prior to deposition. For instance, Volkel and Mahr (2001) report problems with overestimation and underestimation of ages from polymineral fine-grained samples, caused by gelifluction or pedo/bioturbation. In particular, the primary slope sediments in basal layer may hold only autochthonous material, poorly or non-bleached at all (Hülle et al., 2009).

All younger luminescence ages obtained in this study relate to MIS 2 and the transition to MIS 1 (Holocene). Three ages between c. 17–20 ka group to the late LGM and the transition to the Late Glacial. They indicate marked mineral dust sedimentation or reworking of loess deposits along the slope during this period. The two youngest ages corresponding to late MIS 2 and most likely to the Younger Dryas (YD; 12.68–11.59 ka, Litt et al., 2003) although the errors of the luminescence ages reach into Holocene at S3 and Bølling/Allerød at S4. For the latter profile, this young luminescence age for the aeolian cover supports the assumption that this layer is not the remnant of a thick loess cover from the LGM, as we assumed initially. Our luminescence ages for the upper layers stand well with ages given by Hülle et al., (2009), which provide very consistent data pointing on Younger Dryas as a depositional time of the upper layers. These processes of LH formation might reach even Early Holocene as it was postulated by Veit et al. (2017).

The two oldest luminescence ages are from profile S2, but they have to be regarded as minimum ages, because the fading corrected natural IRSL intensity for these two samples are indistinguishable from the signal saturation level. They point to at least Middle Pleistocene age of the silt-textured deposits (3Btg) below the (reworked) glacio-fluvial deposits (2Btg). The lower part of profile S2 (5BC horizon) represents deposits of MIS 10 or older, but it is barely possible to link the sediments to particular glacial or interglacial periods based on one minimum age.

### 4.3. Pedogenesis, and correlations

The luminescence ages provide a chronostratigraphic framework for the polygenetic evolution of the studied soils previously discussed by Waroszewski et al (2018b) in terms of presence of aeolian silts on investigated slopes. The data (OSL ages and micromorphology) allow the correlation of stratigraphic units with geomorphic processes that lead to a complex profile evolution in the interplay of aeolian dust

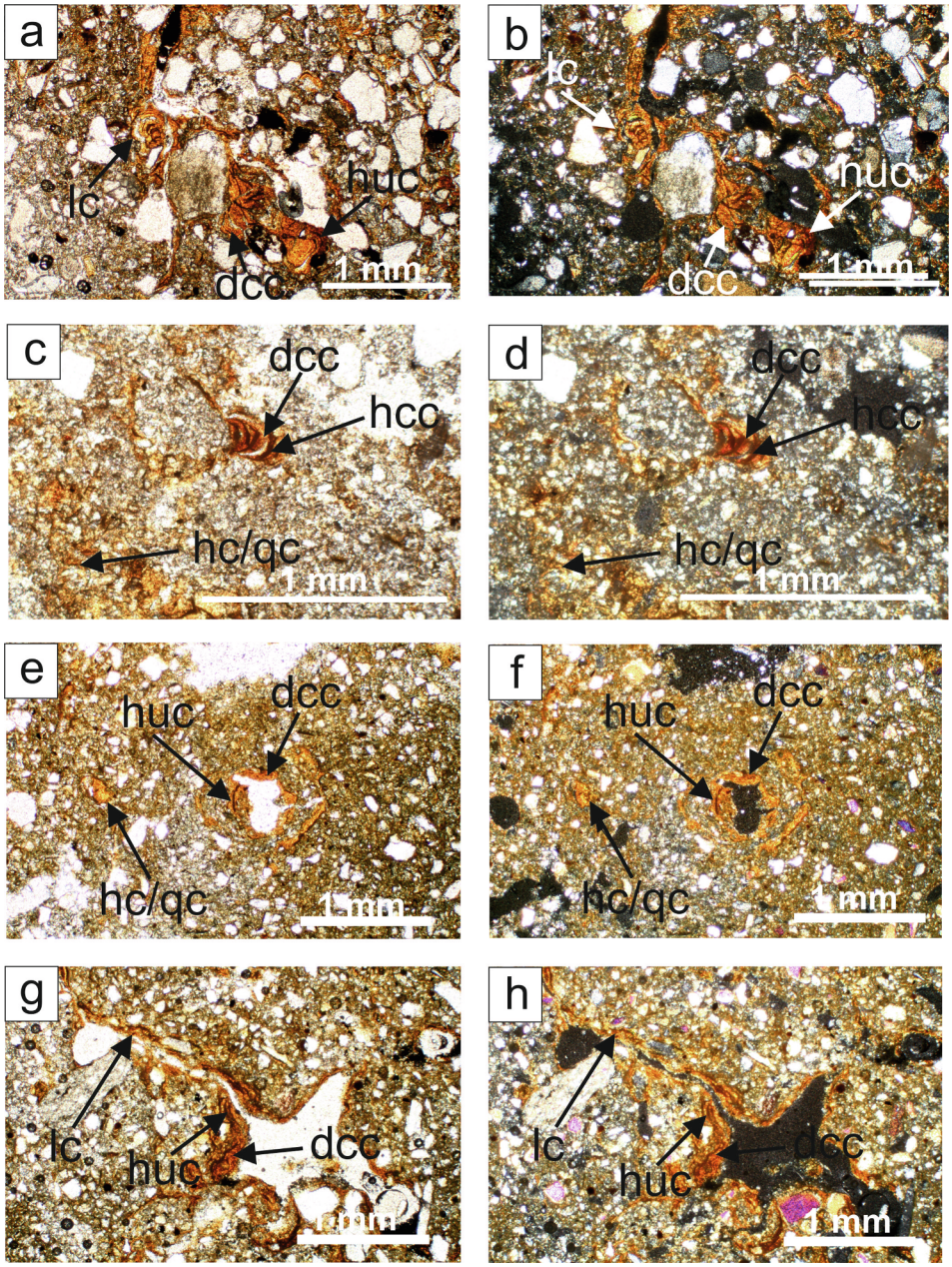


**Fig. 4.** Microphotographs of thin soil sections from profile S2 Btg (a-d) and S2 3Bt (e-h) showing alternating clay coatings. Explanations: (qc/hc) – clay quasi- and hypocoatings, (huc) – humus clay coating, (dcc) – dusty clay coating, (lc) – limpid clay. Bar length = 1 mm. a, c, e, g – PPL microphotographs; b, d, f, g – XPL microphotographs.

accumulation, reworking and pedogenesis.

Profile S2 represents multiple phases of morphodynamic activity and stability due to a high degree of stratification (granite regolith, sandy/gravelly layers, surficial thick loess deposits) but also because of development of different illuvial horizons. The silty-textured horizon below the glacio-fluvial material shows clear alternation of dusty and limpid clay skins (with some humus clay coatings), however with less intense orientation and microlamination comparing with uppermost horizons. These may correspond to the same illuviation as observed in the upper horizons but could also be related to an older phase of pedogenesis. For an independent phase of pedogenesis, testifies a higher weathering degree of the 3Btg horizon compared to the Btg horizon in a similar loess-like materials, indicated mostly by a more intensive speckled b-fabric. This process must have occurred probably before the deposition of the glacio-fluvial material. Moreover, the erosional boundary and no continuation of tongues from the compacted overlying glacio-fluvial layer suggest independent and much earlier clay illuviation. Based on the luminescence data, the parent material of the 3Btg was deposited during the late Middle Pleistocene, but it is difficult to attribute this phase of pedogenesis to a certain time span. There are no absolute ages available for the glacio-fluvial material, the parent material of the 2Btg horizon, but probably it is related to the Odra glaciation (MIS 8/6), the last glacial advance that reached the footslopes of Mt Sleza (Fig. 1). (Micro-)morphological observations for both, the Btg from the overlying loess-like deposits dated to the LGM and the 2Btg horizon developed in the glacio-fluvial deposits show similar types of clay coatings. Despite the old age of the 2Btg parent material, there is no evidence for phases of clay illuviation earlier than the LGM.

The LGM loess deposits in profile S3 showed very comparable effects of pedogenesis with loess mantle in profile S2. Clay coatings in the Btg/Eg of profile S2 are strongly alternating (humus, dusty and limpid partially laminated) and also indicate two phases of clay illuviation. It

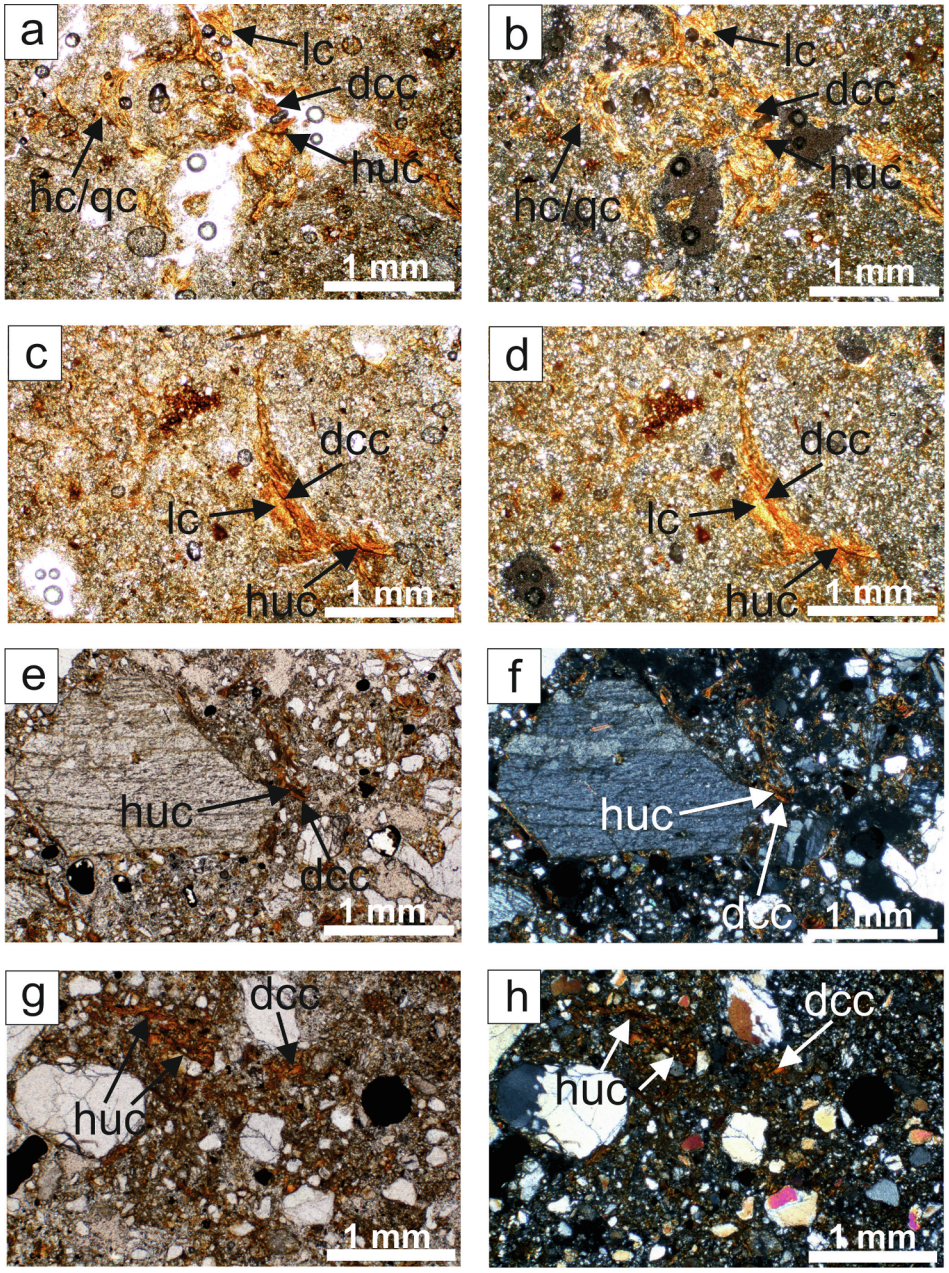


**Fig. 5.** Microphotographs of thin soil sections from profile S3 Btg (a-d) and S4 Bt (e-h) showing alternating (a-d) and fragmented clay coatings (e-h). Explanations: (qc/hc) – clay quasi- and hypocoatings, (huc) – humus clay coating, (dcc) – dusty clay coating, (lc) – limpid clay. Bar length = 1 mm. a, c, e,– PPL microphotographs; b, d, f,– XPL microphotographs.

is not entirely clear whether clay translocation in these two profiles is entirely Holocene or if a previous phase during the Late Glacial needs to be considered. Usually, argic horizons in the region are attributed to the Holocene (Kabala et al., 2015), but we cannot exclude Late Glacial clay translocation as reported for German/England soils/deposits by Büssemer (1994), Catt and Staines (1998) or Kühn and Kösel (2000).

Profile S4 reveals weak and strongly disturbed humus and dusty clay coatings directly below the loess mantle dated to the YD. Their

**Table 3**
Radioactivity data and dose rates.

| Sample | U (ppm) | Th (ppm) | K (%) | Water (%) | Dose rate (Gy/ka) |
|---|---|---|---|---|---|
| LUM3611 | 2.67 ± 0.15 | 9.97 ± 0.54 | 1.82 ± 0.10 | 20 ± 10 | 3.52 ± 0.24 |
| LUM3612 | 2.37 ± 0.13 | 9.49 ± 0.51 | 1.55 ± 0.09 | 20 ± 10 | 3.14 ± 0.23 |
| LUM3613 | 1.64 ± 0.09 | 6.66 ± 0.36 | 1.20 ± 0.07 | 5 ± 5 | 2.72 ± 0.20 |
| LUM3614 | 2.46 ± 0.14 | 7.32 ± 0.40 | 1.60 ± 0.09 | 20 ± 10 | 3.02 ± 0.22 |
| LUM3618 | 2.96 ± 0.17 | 10.25 ± 0.55 | 1.83 ± 0.10 | 20 ± 10 | 3.62 ± 0.24 |
| LUM3619 | 3.04 ± 0.16 | 11.07 ± 0.58 | 1.94 ± 0.11 | 20 ± 10 | 3.83 ± 0.25 |
| LUM3620 | 2.70 ± 0.15 | 8.87 ± 0.46 | 1.76 ± 0.10 | 20 ± 10 | 3.37 ± 0.23 |

**Table 4**
Equivalent dose, fading rate and ages.

| Sample | $D_e$ (Gy) | g-value (%/decade) | Fading uncorrected age (ka) | Fading corrected age (ka) |
|---|---|---|---|---|
| LUM3611 | 62.4 ± 0.4 | 1.1 ± 0.0 | 17.7 ± 1.2 | 19.5 ± 1.3 |
| LUM3612 | 654 ± 11 | 2.4 ± 0.2 | 208 ± 15 | > 280 ± 19 |
| LUM3613 | 666 ± 5 | 2.6 ± 0.2 | 245 ± 18 | > 326 ± 23 |
| LUM3614 | 39.3 ± 0.2 | 1.0 ± 0.2 | 13.0 ± 1.0 | 14.2 ± 1.1 |
| LUM3618 | 59.8 ± 0.3 | 1.2 ± 0.1 | 16.5 ± 1.1 | 18.4 ± 1.2 |
| LUM3619 | 60.4 ± 0.4 | 1.1 ± 0.1 | 15.8 ± 1 | 17.3 ± 1.1 |
| LUM3620 | 36.0 ± 0.3 | 1.1 ± 0.1 | 10.7 ± 0.7 | 12.0 ± 1.0 |

destruction must have occurred before the deposition of the LH. Another option is that the disrupted clay coatings belong to an even earlier phase of pedogenesis, e.g. MIS 3 or the last interglacial. At the present, without further chronological and micromorphological data, we propose three scenarios:

1) Late Glacial clay illuviation: The weak disturbed clay coatings visible in S4 are a relict of Late Glacial pedogenesis. Holocene pedogenesis in acid soil sediment (LH) reworked during the YD did not support additional clay translocation. Late Glacial clay translocation in the profiles S2 and S3 may be as well interrupted during the YD and overprinted by intensive Holocene clay illuviation. Clay translocation in the Late Glacial was confirmed in several location across Northern Hemisphere (eg. Rose et al., 2000), however complete development of Luvisols during that time remains open (e.g. Kühn, 2003; Van Vliet-Lanoe, 1998) as strong proofs for determining main clay illuviation phase are missing and some authors suggest the Early Holocene as starting point of clay migration (Payton, 1992).
2) Holocene clay illuviation: Compared to Western Europe and NE-Germany (Guiot et al., 1993), Poland has a more continental climate, which questions advanced weathering already during the Late Glacial. Besides interglacial Bt horizons of Luvisols, there are no indications for clay translocation in loess-paleosol sequences of SW Poland (Jary, 2010). Kabała et al., (2019) recently discovered Chernozems from loess below earthen burrows of the Funnel Beaker culture in the lowlands near to Mt. Ślęża, having Late Glacial (12670–13000 cal. BP) ages. According to this study, burrow mound soils transformed into Retisols with strong clay illuviation features, but only since the Neolithic (5480–5310 cal. BP). Accordingly, well-developed clay coatings in S2 and S3 result from Holocene pedogenesis and the disturbance of profile S4 is much younger, post-dating Holocene clay translocation. In this case, the luminescence age of LH in profile S4 has to be ignored.
3) Parent material differences: There is no clear evidence for post-sedimentary disturbance from the luminescence data of profile S4. Disturbance by bioturbation would result in much younger ages, but our data make us assume morphodynamic / biogenic stability since the YD. The discrepancy in the models presented above may be related to differences in parent materials. Profile S4 experienced only weak dust accumulation during the Late Glacial, therefore we have to assume a low carbonate content, caused also by strong reworking of primary deposited /admixed loess that might promote and enhanced leaching processes. Late Glacial moisture could have been sufficient to decalcify the local substrate resulting in the mobilization of few clay present within the aeolian admixture. At the same time, the thick loess mantles of profiles S2 and S3 may have experienced only initial decalcification, as clay features are much more pronounced here, and no further chemical weathering.

## 5. Conclusions

In our study we provide and discuss chronological framework for the processes that led to the formation of soils from complex slope deposits with significant loess admixture on Mt. Ślęża. Luminescence ages, micromorphology and granulometry allow linking the age and forming processes of these pedosedimentary records to regional palaeoenvironmental conditions and help to understand the complexity of soil forming processes. The oldest aeolian silt deposits with signs of pedogenesis are of Middle Pleistocene age (> 280 ± 19 ka) and contain a paleosol with more weathered soil mass expressed by well-developed speckled b-fabric. Thick silty slope deposits encompass the maximum loess thickness and are dated to the LGM or slightly younger, while glacio-fluvial sediment is older and supposed to have formed during the penultimate glacial (MIS 6). Luminescence ages from the upper layers of silty mantles indicate shallow reworking, which we tentatively correlate to the Younger Dryas (YD) oscillation. The reliability of the age of the aeolian mantle age in profile S4 decides about the interpretation of the starting point of advanced soil forming processes (clay illuviation). Only the thin loess mantle over granite regolith in profile S4 indicates some weak Late Glacial clay illuviation (probably MIS 2 pedogenesis), while glacio-fluvial and thick loess sediments in profiles S2 and S3 were most likely overprinted by pedogenesis (clay illuviation) during the Holocene. The main period of Luvisol/Alisol formation in our study is most likely the Holocene, not the Late Glacial – only very weak clay illuviation might have occured before the Younger Dryas in exceptional settings (profile S4). The possibility of complete argic horizon formation during the Late Glacial remains open for SW Poland.

**Table 5**
Selected micromorphological features of studied soils.

| Profile/soil horizon | Depth(cm) | Microstructure | Groundmass | | Pedofeatures | | | | | |
|---|---|---|---|---|---|---|---|---|---|---|
| | | | Type | b-fabric | Nodules | Illuvial clay coatings | | | | |
| | | | | | | limpid | dusty clay | humus | layered | distorted |
| S2 Btg | 55–61 | subangular blocky | double spaced porphyric | granostraited, random-striated | anorthic iron hydroxide nodules | +/++ | + | (+)/+ | + | – |
| S2 3Btg | 111–117 | subangular blocky | single spaced porphyric | random-striated, circular-striated, granostriated, | anorthic iron hydroxide nodules | +/++ | (+)/+ | (+) | (+)/+ | – |
| S3 Btg/Eg | 74–80 | subangular blocky | fine monic | crescent striated, random-striated, granostriated | anorthic iron hydroxide nodules | ++ | + | (+) | (+)/+ | – |
| S4 2Bt | 24–30 | crumby | single spaced porphyric | random-striated, granostriated, porostrated | anorthic iron hydroxide nodules | – | +/++ | (+)/+ | (+) | ++ |

Explanation: (+) – < 2% (< 5% for fabric units), + – 2% (5% for fabric units), ++ – 2–5% (5–15% for fabric units).

## Declaration of Competing Interest

The authors declared that there is no conflict of interest.

## Acknowledgements

This research was financed by National Science Center (Poland) project Sonata 8 No 2014/15/D/ST10/04087 (awarded to Jaroslaw Waroszewski) and NAWA PROM programme PPI/PRO/2018/1/00004/U/001 (awarded to Tobias Sprafke). Małgorzata Kamińska and Janusz Kamiński are acknowledged for their help during field works. We thank Ryszard Mazurek and Joanna Kowalska for their support in thin sections preparation and three anonymous reviewers who helped to improved the final version of the manuscript.

## References

Auclair, M., Lamothe, M., Huot, S., 2003. Measurement of anomalous fading for feldspar IRSL using SAR. Radiat. Meas. 37, 487–492.
Badura, J., Jary, Z., Smalley, I., 2013. Sources of loess material for deposits in Poland and part of Central Europe: the lost Big River. Quat. Int. 296, 15–22.
Bussemer, S., 1994. Geomorphologische und bodenkundliche Untersuchungen an periglaziaren Deckserien des mittleren und ostlichen Barnim. Berl. Geogr. Arb. 80, 150 pp. (Berlin).
Bussemer, S., 2002. Periglacial cover-beds in the young moraine landscapes of northern Eurasia. Z. Geomorph. N.E. Suppl.-Bd.127, 81-105.
Catt, J.A., Staines, S.J., 1998. Petrography of sediments and buried soils. In: Preece, R.C., Bridgland, D.R. (Eds.), Late Quaternary Environmental Change in North-west Europe: Excavations at Holywell Coombe, South-east England. Chapman & Hall, London, pp. 69–85.
Costantini, E.A.C., Priori, S., 2007. Pedogenesis of plinthite during early Pliocene in the Mediterranean environment. Case study of a buried paleosol at Podere Renieri, central Italy. Catena 71, 425–443.
Döhlert, S., Terhorst, B., Frechen, M., Zhang, J., Damm, B., 2018. Chronostratigraphic interpretation of intermediate layer formation cycles based on OSL -dates from intercalated slope sediments. Catena 162, 278–290.
Frechen, M., Boenigk, W., Weidenfeller, M., 1995. Chronostratigraphie des 'Eiszeitlichen Lossprofils' in Koblenz-Metternich. Mainzer Geowiss. Mitt. 24, 155–180.
Fuchs, M., Lang, A., 2009. Luminescence dating of hillslope deposits—A review. Geomorphology 109 (1), 17–26.
Gild, C., Geitner, C., Sanders, D., 2018. Discovery of a landscape-wide drape of lateglacial aeolian silt in the western Northern Calcareous Alps (Austria): first results and implications. Geomorphology 301, 39–52. https://doi.org/10.1016/J.GEOMORPH.2017.10.025.
Guerin, G., Mercier, N., Adamiec, G., 2011. Doseerate conversion factors: update. Anc. TL 29, 5–8.
Guiot, J., de Beaulieu, J.L., Cheddadi, R., David, F., Ponel, P., Reille, M., 1993. The climate in Western Europe during the last Glacial/Interglacial cycle derived from pollen and insect remains. Palaeogeogr. Palaeoclimatol. Palaeoecol. 103 (1–2), 73–93.
Hall, A.M., Migoń, P., 2010. The first stages of erosion by ice sheets: evidence from central Europe. Geomorphology 123, 349–363.
Huntley, D.J., Lamothe, M., 2001. Ubiquity of anomalous fading in K- feldspars and the measurment and correction for it in optical dat- ing. Can. J. Earth Sci. 38 (7), 1039–1106.
Hülle, D., Hilgers, A., Kühn, P., Radtke, U., 2009. The potential of optically stimulated luminescence for dating periglacial slope deposits — a case study from the Taunus area, Germany. Geomorphology 109, 66–78.
IUSS Working Group WRB, 2015. World Reference Base for Soil Resources 2014, update 2015 International Soil Classification System for Naming Soils and Creating Legends for Soil Maps. World Soil Resources Reports No. 106. FAO, Rome.
Jary, Z., Kida, J., Snihur, M., 2002. Lessy i osady lessopochodne w południowo-zachodniej Polsce. Czasopismo Geograficzne 1 (73), 63–100.
Kabala, C., Jezierski, P., 2011. Geography, morphology, climate and soils of the Lower Silesia. IUSS Working group WRB field guide. Workshop and Field Excursion. Wroclaw-Karpacz, Wroclaw University of Environmental and Life Sciences.
Kabała, C., Przybył, A., Krupski, M., Łabaz, B., Waroszewski, J., 2019. Origin, age and transformation of Chernozems in northern Central Europe – new data from Neolithic earthen barrows in SW Poland. Catena 180, 83–102.
Kacprzak, A., Derkowski, A., 2007. Cambisols developed from cover-beds in the Pieniny Mts (southern Poland) and their mineral composition. Catena 71, 292–297.
Kars, R.H., Wallinga, J., Cohen, K.M., 2008. A new approach towards anomalous fading correction for feldspar IRSL datingetests on samples in field saturation. Radiat. Meas. 43 (2e6), 786e790.
Kida, J., 1999. Stan badań lessów i osadów lessopodobnych na obszarze Dolnego Śląska. In: Jary, Z. (Ed.), III Seminarium Lessowe – Geneza i wiek pokrywowych utworów pylastych południowo-zachodniej Polski. Uniwersytet Wrocławski, Wrocław-Bożków, Poland, pp. 43–54.
Kleber, A., 1997. Cover-beds as soil parent materials in midlatitude regions. Catena 30, 197–213. https://doi.org/10.1016/S0341-8162(97)00018-0.
Kleber, A., Dietze, M., Terhorst, B., 2013. Sedimentary properties of layers. In: Kleber, A., Terhorst, B. (Eds.), Mid-Latitude Slope Deposits (Cover-Beds). Developments in Sedimentology 66 Elsevier, pp. 12–18.
Kleber, A., Terhorst, B., 2013. Mid-latitude slope deposits (cover beds) developments in sedimentology. Elsevier 66, 302.
Konert, M., Vandenberghe, J.E.F., 1997. Comparison of Laser Grain Size Analysis with Pipette and Sieve Analysis: A Solution for the Underestimation of the Clay Fraction. Sedimentology 44, 523–535. https://doi.org/10.1046/j.1365-3091.1997.d01-38.x.
Kowalska, J.B., Zaleski, T., Józefowska, A., Mazurek, R., 2019. Soil formation on calcium carbonate-rich parent material in the outer Carpathian Mountains – A case study. Catena 174, 436–451.
Kryza, R., Pin, C., 2010. The central-sudetic ophiolites (SW Poland): petrogenetic issues, geochronology and palaeotectonic implications. Gondwana Res. 17, 292–305.
Kühn, P., 2003. Micromorphology and late glacial/holocene genesis of luvisols in mecklenburg-vorpommern (NE-Germany). Catena 54, 537–555.
Kühn, P., Kösel, M., 2000. Spatglaziale boden-und substratgenese: mikromorphologisch stratigraphische befunde aus dem su¨dwestdeutschen alpenvorland. Trierer Bodenk. Schr. 1, 51–57.
Lamothe, M., Auclair, M., Hamzaoui, C., Huot, S., 2003. Towards a prediction of long-term anomalous fading of feldspar IRSL. Radiat. Meas. 37 (4–5), 493–498.
Li, Y., Tsukamoto, S., Long, H., Zhang, J., Yang, L., He, Z., Frechen, M., 2018. Testing the reliability of fading correction methods for feldspar IRSL dating: a comparison between natural and simulated-natural dose response curves. Radiat. Meas. 120, 228–233.
Litt, T., Schmincke, H.-U., Kromer, B., 2003. Environmental response to climatic and volcanic events in central Europe during the Weichselian Lateglacial, Quaternary Sci. Rev. 22, 7–32.
Loba, A., Sykuła, M., Kierczak, J., Łabaz, B., Bogacz, A., Waroszewski, J., 2020. In situ weathering of rocks or an eolian silt deposition: key parameters for veryfing parent material and pedogenesis in the Opawskie Mountains - a case study from SW Poland. J. Soils Sediments 20, 435–451.
Kabala, C., Bekier, J., Bińczycki, T., Bogacz, A., Bojko, O., Cuske, M., Ćwieląg-Piasecka, I., Dębicka, M., Gałka, B., Gersztyn, L., Glina, B., Jamroz, E., Jezierski, P., Karczewska, A., Kaszubkiewicz, J., Kawałko, D., Kierczak, J., Kocowicz, A., Krupski, M., Kusza, G., Łabaz, B., Marzec, M., Medyńska-Juraszek, A., Musztyfaga, E., Perlak, Z., Pędziwiatr, A., Pora, E., Przybył, A., Strączyńska, S., Szopka, K., Tyszka, R., Waroszewski, J., Weber, J., Woźniczka, P., 2015. Soils of Lower Silesia: Origins, Diversity and Protection. PTG. PTSH, Wrocław (256 pp.).
Lorz, C., Frühauf, M., Mailänder, R., Phillips, J.D., Kleber, A., 2013. Influence of cover beds on soils. In: Kleber, A., Terhorst, B. (Eds.), Mid-Latitude Slope Deposits (Cover-Beds). Developments in Sedimentology. 66. pp. 95–125.
Labaz, B., Musztyfaga, E., Waroszewski, J., Bogacz, A., Jezierski, P., Kabala, C., 2018. Landscape-related transformation and differentiation of Chernozems — catenary approach in the Silesian Lowland. SW Poland. Catena 161. https://doi.org/10.1016/j.catena.2017.10.003.
Labaz, B., Kabala, C., Waroszewski, J., 2019a. Ambient geochemical baselines for trace elements in Chernozems—approximation of geochemical soil transformation in an agricultural area. Environ. Monit. Assess. 191, 19.
Łabaz, B., Kabała, C., Dudek, M., Waroszewski, J., 2019b. Morphological diversity of chernozemic soils in south-western Poland. Soil Science Annual 70 (3), 211–222.
Martignier, L., Nussbaumer, M., Adatte, T., Gobat, J.-M., Verrecchia, E.P., 2015. Assessment of a locally-sourced loess system in Europe: the Swiss Jura Mountains. Aeolian Res. 18, 11–21. https://doi.org/10.1016/J.AEOLIA.2015.05.003.
Mailänder, R., Veit, H., 2001. Periglacial cover-beds on the Swiss Plateau: indicators of soil, climate and landscape evolution during the Late Quaternary. Catena 45, 251–272.
Migoń, P., Kacprzak, A., 2014. Lateral diversity of regolith and soils under a mountain slope — implications for interpretation of hillslope materials and processes, central Sudetes, SW Poland. Geomorphology 221, 69–82.
Migoń P., 1997. Crystalline Rock Inselbergs in Southwestern Poland. Origin and Palaeoenvironmental Significance, Acta Universitatis Wratislaviensis No 1872, Studia Geograficzne, LXVI.
Murray, A.S., Wintle, A.G., 2000. Luminescence dating of quartz using improved single aliquot regenerative-dose protocol. Radiat. Meas. 32, 57–73.
Murray, A.S., Wintle, A.G., 2003. The single aliquot regenerative dose protocol: potential for improvements in reliability. Radiat. Meas. 37, 377–381.
Payton, R.W., 1992. Fragipan formation in Argillic brown earths (Fragiudalfs) of the Milfield Plain, north-east England: I. Evidence for a periglacial stage of development. J. Soil Sci. 43, 621–644.
Phillips, J.D., 2010. The convenient fiction of steady state soil thickness. Geoderma 156 (3–4), 389–398.
Pędziwiatr, A., Kierczak, J., Waroszewski, J., Ratié, G., Quantin, C., Ponzever, E., 2018. Rock-type control of Ni, Cr, and Co phytoavailability in ultramafic soils. Plant Soil 423, 339–362.
Prescott, J.R., Hutton, J.T., 1994. Cosmic ray contributions to dose rates for luminescence and ESR dating: large depths and longeterm time variations. Radiat. Meas. 23, 497–500.
Rees-Jones, J., 1995. Optical dating of young sediments using fine-grain quartz. Ancient TL 13, 9–14.
Roberts, H.M., 2008. The development and application of luminescence dating to loess deposits: a perspective on the past, present and future. Boreas 37, 483–507. https://doi.org/10.1111/j.1502-3885.2008.00057.
Rose, J., Lee, J.A., Kemp, R.A., Harding, P.A., 2000. Palaeoclimate, sedimentation and soil development during the Last Glacial Stage (Devensian), Heathrow Airport, London UK. Quat. Sci. Rev. 19, 827–847.
Schaetzl, R.J., Luehmann, M.D., 2013. Coarse-textured basal zones in thin loess deposits: products of sediment mixing and/or paleoenvironmental change? Geoderma 192,

277–285. https://doi.org/10.1016/J.GEODERMA.2012.08.001.
Schmincke, H.-U., 2006. Environmental impacts of the Lateglacial eruption of the Laacher See Volcano, 12.900 cal BP. In: von Königswald, W., Litt, T. (Eds.), 150 years of Neanderthal Discoveries. Terra Nostra, 2006/2. Bonn, Germany, pp. 149–153.
Schulte, P., Lehmkuhl, F., Steininger, F., Loibl, D., Lockot, G., Protze, J., Fischer, P., Stauch, G., 2016. Influence of HCl pretreatment and organo-mineral complexes on laser diffraction measurement of loess-paleosol-sequences. Catena 137, 392–405.
Schulte, P., Sprafke, T., Rodrigues, L., Fitzsimmons, K.E., 2018. Are fixed grain size ratios useful proxies for loess sedimentation dynamics? Experiences from Remizovka, Kazakhstan. Aeolian Res. 31, 131–140.
Semmel, A., Terhorst, B., 2010. The concept of Periglacial cover beds in central Europe: a review. Quat. Int. 222, 120–128.
Sprafke, T., Thiel, C., Terhorst, B., 2014. From micromorphology to palaeoenvironment: the MIS 10 to MIS 5 record in Paudorf (Lower Austria). Catena 117, 60–72.
Sprafke, T., 2016. Löss in Niederösterreich - Archiv quartärer Klima- und Landschaftsveränderungen. Würzburg University Press, Würzburg, pp. 272.
Stockmann, U., Minasny, B., McBratney, A.B., 2014. How fast does soil grow? Geoderma 216, 48–61.
Stoops, G., 2003. Guidelines for analysis and description of soil and regolith thin section. Soil Science Society of America Inc, Madison, Wisconsin, USA.
Thomsen, K.J., Murray, A.S., Jain, M., Bøtter-Jensen, L., 2008. Laboratory fading rates of various luminescence signals from feldspar-rich sediment extracts. Radiat. Meas. 43, 1474–1486.
Veit, H., Trauerstein, M., Preusser, F., Messmer, T., Gnägi, C., Zech, R., Wüthrich, L., 2017. Late Glacial/Early Holocene slope deposits on the Swiss Plateau: genesis and palaeo-environment. Catena 158, 102–112.
Van Reeuwijk, L.P., 2002. Procedures for Soil Analysis, 6th ed. ISRIC, Wageningen, Netherlands.
Van Vliet-Lanoë, B., 1998. Frost and soils: implications for paleosols, paleo-climates and stratigraphy. Catena 34, 157–183.
Techmer, A., Rolf, C., Weidenfeller, M., 2006. Lumineszenz-Chronologie und paläomagnetische Untersuchungen des Lößprofils Alsheim (Mainzer Becken). Mainzer geowiss. Mitt. 34, 113–134.
Waroszewski, J., Kalinski, K., Malkiewicz, M., Mazurek, R., Kozlowski, G., Kabala, C., 2013. Pleistocene-Holocene cover-beds on granite regolith as parent material for Podzols — an example from the Sudeten Mountains. Catena 104, 161–173.
Waroszewski, J., Sprafke, T., Kabala, C., Musztyfaga, E., Labaz, B., Wozniczka, P., 2018a. Aeolian silt contribution to soils on the mountain slopes (Mt. Ślęża, SW Poland). Quat. Res. 89 (3), 702–717.
Waroszewski, J., Egli, M., Brandová, D., Christl, M., Kabala, C., Malkiewicz, M., Kierczak, J., Glina, B., Jezierski, P., 2018b. Identifying slope processes over time and their imprint in soils of medium-high mountains of Central Europe (the Karkonosze Mountains, Poland). Earth Surf. Process. Landf. 43 (6), 1195–1212.
Waroszewski, J., Sprafke, T., Kabala, C., Kobierski, M., Kierczak, J., Musztyfaga, E., Łabaz, B., 2019. Tracking textural, mineralogical and geochemical signatures in soils developed from basalt-derived materials covered with loess sediments (SW Poland). Geoderma 337, 983–997.
Wintle, A.G., 1973. Anomalous fading of thermoluminescence in mineral samples. Nature 245, 143–144.
Wintle, A.G., Murray, A.S., 2006. A review of quartz optically stimulated luminescence characteristics and their relevance in single-aliquot regeneration dating protocols. Radiat. Meas. 41, 369–391.
Volkel, J., Mahr A., 2001. Die ISRL-Datierung von periglazialen Hangsedimenten – Ergebnisse aus dem Bayerischen Wald. Z .Geomorph. N.F. 45, 285-305.
Zerboni, A., Trombino, L., Frigerio C., Livio, F., Berlusconi A., Michetti A.M., Rodnight H., Spotl, C., 2014. The loess-paleosol sequence at Monte Netto: a record of climate change in the Upper Pleistocene of central Po Plain, northern Italy.
Żurawek, R., 1999. Geochemiczne kryterium allochtoniczności drobnych frakcji w pokrywach stokowych Masywu Ślęży. [In Polish.] In Jary, Z. (Ed.), III Seminarium Lessowe – Geneza i wiek pokrywowych utworów pylastych południowo-zachodniej Polski. Wrocław-Bożków, pp. 77–81.
Żurawek, R., 2001. Problem wieku reliktowych lodowców skalnych w Masywie Ślęży w świetle datowań 14C i OSL oraz obserwacji geomorfologicznych. Przegląd Geologiczny 49, 10/1, 880-884.